Low-Velocity Impact Response of Laminated Beams Subjected to Initial Stresses

Bhavani V. Sankar*
Bradley University, Peoria, Illinois
and
C.T. Sun†
Purdue University, West Lafayette, Indiana

Finite element procedures are used in conjunction with a numerical algorithm to compute the impact response of a graphite-epoxy laminated beam subjected to tensile initial stresses. The effect of initial stresses on the contact duration, impact force, coefficient of restitution, and bending and shear stresses are discussed. The analytically computed contact force history and strain response are compared with some experimental results.

Introduction

DURING the past decade foreign object impact damage to composites has received a great deal of attention. Although the failure process is expected to involve only fundamental mechanisms such as matrix cracking, fiber rupture, delamination, and local plastic deformation, an analytical prediction methodology that includes initiation, development, and termination of the failure process has not yet evolved; in fact, it is formidable. Nevertheless, several attempts have been made to understand impact damage in composites that have met with limited success.[1] A meaningful impact response analysis requires a good estimate of contact force throughout the impact duration. Low-velocity impact problems, which also took the local indentation into account, have been solved by several authors.[2-5] This approach requires a knowledge of contact laws that, in the case of composite laminates, are obtained from static indentation tests.[6]

In most of the above studies it was assumed that the impacted structure was free of any initial stresses. But, in practice, the composite facing of a structure may be under a preload (e.g., a sandwich structure with laminate facing under bending loads, jet engine fan blades subjected to centrifugal forces), which may aggravate the damage due to impact. So, it is imperative that the effect of initial stresses be considered in impact problems. Very few works have reported on the impact damage of composites under initial stresses.[7,8] Sun and Chattopadhyay[9] studied the impact response of initially stressed laminated plates using the modal expansion method. They found that tensile initial stresses tend to increase the magnitude of contact force, but reduce the contact time, plate deflection, and the incremental stresses due to impact. It was also noted that a higher preload results in less energy transfer from the striking mass to the plate. The results obtained in the above study were of a general nature. So, it was decided to conduct further studies with a particular material system (graphite-epoxy laminates) and for a given range of impact velocity and preload.

In this study, an efficient numerical algorithm developed by the authors[10] has been used to compute the impact response. A plane strain rectangular finite element with higher-order degrees of freedom has been used to compute the generic S and S^e functions required in the impact analysis. The effect of initial stresses on the contact duration, impact force, coefficient of restitution, and bending and shear stresses are discussed. In addition, low-velocity impact tests were conducted using a force transducer as a pendulous impactor. The target was a graphite-epoxy laminated beam. In some of the impact tests, the beam was under tensile initial stresses. The experimental impact force history and strain response are compared with the analytical results.

Impact Analysis

A Numerical Algorithm

The details of this numerical method, criteria for selecting the time increment Δt, and efficiency of computation have been discussed in Ref. 10. For the sake of completeness, a brief account of the method is given here.

Assume a rigid mass m impacts a structure with a velocity v. The equation of motion of the impactor can be written as

$$m\ddot{\chi} = -F(t) \tag{1}$$

where χ is the displacement of the impactor and $F(t)$ the contact force. The double dots denote the second derivative with respect to time. The normal displacement of the structure at the impact point $w(t)$ can be written as

$$w(t) = \int_0^t F(\tau)\, g(t-\tau)\, \mathrm{d}\tau \tag{2}$$

where $g(t)$ is the dynamic Green's function for the w displacement. The local indentation α is defined as

$$\alpha(t) = \chi(t) - w(t) \tag{3}$$

The relation between contact force and the indentation is assumed to be of the form

$$F = k\alpha^n \tag{4}$$

where k and n are found from static indentation tests.[6]

We shall assume that the contact force variation is linear in time during each small time increment Δt. Thus,

$$F(t) = \sum_{i=0,1,2\ldots} q_i R\langle t - i\,\Delta t\rangle \tag{5}$$

Received Sept 6, 1984; revision received March 4, 1985.

*Assistant Professor of Mechanical Engineering. Member AIAA.
†Professor of Aeronautics and Astronautics. Associate Fellow AIAA.

where the q_i are the unknowns that decide the contact force history and $R\langle\ \rangle$ is a function in time defined as

$$\begin{aligned} R\langle t-t_0\rangle &= 0, \quad 0 \le t \le t_0 \\ &= (t-t_0)/\Delta t, \quad t_0 \le t \le t_0+\Delta t \\ &= 1, \quad t > t_0+\Delta t \end{aligned} \tag{6}$$

Substitution of Eq. (5) in Eq. (2), after some simplifications, yields

$$w(t) = \sum_{i=0,1,2\ldots} q_i H\langle t-i\Delta t\rangle S(t-i\Delta t) \tag{7}$$

where

$$S(t) = \int_0^t R(\tau)\, g(t-\tau)\, d\tau \tag{8}$$

and $H\langle t\rangle$ is the Heaviside unit function.

It should be noted that $S(t)$ is the w response of the structure at the impact point due to the load $R\langle t\rangle$. Since $S(t)$ depends only on the given structure, it is seen from Eq. (7) that $w(t)$ has been expressed as a linear function of the unknown q_i.

From Eqs. (1), (5), and (7), we can write the expressions for the contact force, velocity, and displacements at any time $t = i\Delta t$ as

$$\begin{aligned} F_i &= q_0 + q_1 + q_2 + \cdots + q_{i-1} = F_{i-1} + q_{i-1} \\ v_i &= v_{i-1} - F_{i-1}\Delta t/m - q_{i-1}\Delta t/2m \\ \chi_i &= \chi_{i-1} + v_{i-1}\Delta t - F_{i-1}(\Delta t)^2/2m - q_{i-1}(\Delta t)^2/6m \\ w_i &= q_0 S_i + q_1 S_{i-1} + q_2 S_{i-2} + \cdots + q_{i-1} S_1 \end{aligned} \tag{9}$$

In the above expressions, v_i is the velocity of the impactor at $t = i\Delta t$ and $S_i = S(i\Delta t)$. Using Eqs. (9), Eqs. (3) and (4) can be written as

$$\alpha_i = \chi_i - w_i$$

or

$$\left[(F_{i-1} + q_{i-1})/k\right]^{1/n} = C_i - q_{i-1}\left[S_1 + (\Delta t)^2/6m\right] \tag{10}$$

where

$$\begin{aligned} C_i &= \chi_{i-1} + v_{i-1}\Delta t - F_{i-1}(\Delta t)^2/2m \\ &\quad -(q_0 S_i + q_1 S_{i-1} + \cdots + q_{i-2} S_2) \end{aligned}$$

Equation (10) is a nonlinear algebraic equation in the unknown q_{i-1} that can be solved by a simple iterative scheme. Once q_{i-1} is known, Eq. (9) is used to compute the force, velocity, and displacements.

If one is interested in the response of the structure such as stress, strain, or displacement at a particular point, it can be obtained by following the steps used in deriving Eq. (7). For example, it can be shown that the strain response $e(t)$ due to impact is given by

$$e(t) = \sum_{i=0,1,2\ldots} q_i H\langle t-i\Delta t\rangle S^e(t-i\Delta t)$$

where $S^e(t)$ is the strain response due to the load $R\langle t\rangle$.

Finite Element Procedures

As discussed above, the only information we need about the impacted structure is the response to the load $R\langle t\rangle$. The laminated beam was modeled by finite elements that can also account for the initial stresses. The load $R\langle t\rangle$ was applied as a concentrated load at the impact point, and the stresses and displacements at various points of interest were computed and stored on a magnetic tape. Later they were used to compute the impact response for various impact velocities.

The finite element described here is a higher-order rectangular plane strain element to model beam-like structures only. The longitudinal axis of the beam is parallel to the x axis. The four corner nodes have the degrees of freedom u, v, $\partial u/\partial x$, and $\partial v/\partial x$ (see Fig. 1). Here, u represents the displacement in the x direction and v is the y displacement. The shape functions are chosen in such a way that u and v vary as cubic polynomials along the x direction, and their variation in the y direction is linear. The interpolation functions for u and v are given below. For the sake of convenience, normalized variables $r = x/\ell$ and $s = y/b$ are introduced. Note that the finite element is assumed to be a rectangle of size $2\ell \times 2b$.

$$\begin{aligned} u(r,s) &= f_1(r)[u_1 g_1(s) + u_4 g_2(s)] \\ &\quad + f_2(r)[u_2 g_1(s) + u_3 g_2(s)] \\ &\quad + f_3(r)[\ell e_1 g_1(s) + \ell e_4 g_2(s)] \\ &\quad + f_4(r)[\ell e_2 g_1(s) + \ell e_3 g_2(s)] \end{aligned}$$

$$\begin{aligned} v(r,s) &= f_1(r)[v_1 g_1(s) + v_4 g_2(s)] \\ &\quad + f_2(r)[v_2 g_1(s) + v_3 g_2(s)] \\ &\quad + f_3(r)[\ell\theta_1 g_1(s) + \ell\theta_4 g_2(s)] \\ &\quad + f_4(r)[\ell\theta_2 g_1(s) + \ell\theta_3 g_2(s)] \end{aligned}$$

where

$$\begin{aligned} f_1(r) &= \tfrac{1}{4}(1-r)^2(2-r), & f_2(r) &= \tfrac{1}{4}(1+r)^2(2-r) \\ f_3(r) &= \tfrac{1}{4}(1-r)^2(1+r), & f_4(r) &= -\tfrac{1}{4}(1+r)^2(1-r) \\ g_1(s) &= (1-s)/2, & g_2(s) &= (1+s)/2 \end{aligned}$$

In the above expressions, e and θ refer to $\partial u/\partial x$ and $\partial v/\partial x$, respectively.

From the above interpolation functions, some observations regarding interelement compatability can be made. Along a side parallel to the x axis, say side 1-2 (see Fig. 1), all the four nodal degrees of freedom are continuous across the element boundary 1-2. But, the derivatives $\partial u/\partial y$ and $\partial v/\partial y$ are not continuous and, in fact, they need not be if side 1-2 is the boundary between elements of different materials. Along a side parallel to the y axis, say 1-4, u, v, and all their first derivatives are continuous across the element boundary. This

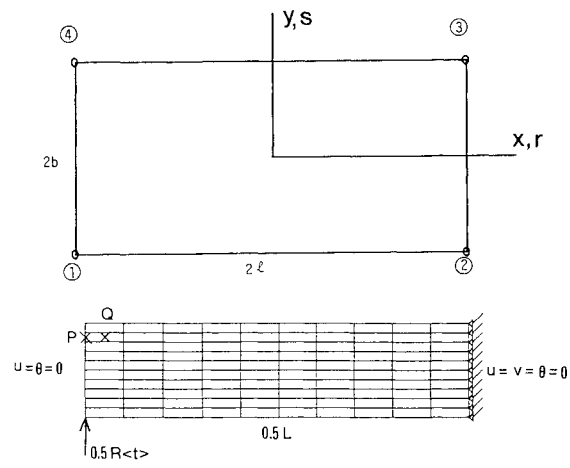

Fig. 1 Plane strain finite element and finite element model of one-half of the beam.

is permissible and also desirable, because side 1-4 is a boundary between elements of the same layer in the laminate.

Stiffness and Mass Matrices

The derivation of element stiffness and mass matrices follows the principles explained in Ref. 11. The interpolation functions given above can be written as

$$\boldsymbol{u}(x,y) = \begin{Bmatrix} u \\ v \end{Bmatrix} = \boldsymbol{N}\boldsymbol{a}^e \tag{11}$$

where $\boldsymbol{a}^e$ is given by

$$\boldsymbol{a}^{eT} = \lfloor u_1 v_1 e_1 \theta_1 u_2 \ldots \theta_3 u_4 v_4 e_4 \rfloor$$

and $\boldsymbol{N}$ is the matrix of shape functions. When there are no initial stresses present, we use the strain-displacement relations of linear elasticity theory, and the element strains are

$$\boldsymbol{\epsilon} = \begin{Bmatrix} \epsilon_{xx} \\ \epsilon_{yy} \\ \gamma_{xy} \end{Bmatrix} = \boldsymbol{B}\boldsymbol{a}^e \tag{12}$$

Matrix $\boldsymbol{B}$ contains the functions $f_1, f_2, \ldots, g_1, g_2$ and their derivatives $f_1', f_2', \ldots, g_1', g_2'$ (a prime indicates differentiation with respect to the argument). We assume a linear elasticity matrix such as

$$\boldsymbol{\sigma} = \begin{Bmatrix} \sigma_{xx} \\ \sigma_{yy} \\ \tau_{xy} \end{Bmatrix} = \boldsymbol{D}\boldsymbol{\varepsilon} \tag{13}$$

By using the standard procedures in Ref. 11, the element stiffness matrix is derived as

$$\boldsymbol{K}^e = \int_{-b}^{+b}\int_{-\ell}^{+\ell} \boldsymbol{B}^T\boldsymbol{D}\boldsymbol{B}\,\mathrm{d}x\,\mathrm{d}y \tag{14}$$

The mass matrix is given by

$$\boldsymbol{M}^e = \rho\int_{-b}^{+b}\int_{-\ell}^{+\ell} \boldsymbol{N}^T\boldsymbol{N}\,\mathrm{d}x\,\mathrm{d}y \tag{15}$$

where ρ is the mass density.

Initial Stress Matrix

In order to study the effect of initial stresses, one has to take the geometric nonlinearities into account. This is achieved by including the nonlinear terms in the strain-displacement relations as follows:

$$\epsilon_{xx} = \frac{\partial u}{\partial x} + \frac{1}{2}\left(\frac{\partial u}{\partial x}\right)^2 + \frac{1}{2}\left(\frac{\partial v}{\partial x}\right)^2, \text{ etc.} \tag{16}$$

It is assumed that the incremental stresses and incremental strains are related by the same elasticity matrix $\boldsymbol{D}$ as before. Now, the stiffness matrix consists of two parts and is given as

$$\boldsymbol{K} = \boldsymbol{K}_0 + \boldsymbol{K}_\sigma \tag{17}$$

in which $\boldsymbol{K}_0$ represents the small-displacement stiffness matrix given by Eq. (12). $\boldsymbol{K}_\sigma$ is known as the initial stress matrix.[11] When the only initial stress component present is $\sigma_{xx}^0 = S^0$, the initial stress matrix is found to be

$$\boldsymbol{K}_\sigma = S^0\int_{-b}^{+b}\int_{-\ell}^{-\ell} (\boldsymbol{P}^T\boldsymbol{P} + \boldsymbol{Q}^T\boldsymbol{Q})\,\mathrm{d}x\,\mathrm{d}y \tag{18}$$

$\boldsymbol{P}$ and $\boldsymbol{Q}$ are defined by the relations

$$\frac{\partial u}{\partial x} = \boldsymbol{P}^T\boldsymbol{a} \text{ and } \frac{\partial v}{\partial y} = \boldsymbol{Q}^T\boldsymbol{a} \tag{19}$$

and can be derived from $\boldsymbol{N}$. The details of derivation are given in Ref. 12. It may be noted that $\boldsymbol{K}_\sigma$ is a constant matrix that depends only on the initial stress S^0 and the dimensions of the element.

Dynamic Analysis

The equation of motion for the finite element assemblage is

$$\boldsymbol{M}\ddot{\boldsymbol{a}} + \boldsymbol{K}\boldsymbol{a} = \boldsymbol{R}(t) \tag{20}$$

where $\boldsymbol{R}$ is the external load vector. The Wilson-θ method was used to perform the direct integration of the above equation. The computer program organization essentially followed the procedures explained in Ref. 13. The performance of the present finite element in static and dynamic loading was evaluated by comparing with some known results.[12]

The finite element mesh for the present impact problem is shown in Fig. 1. It models a clamped-clamped, graphite-epoxy, laminated beam of layup $[0_2/90_2/0_2/90_2/0_2]_s$. Due to the symmetry, one-half of the beam has been modeled. The impact is assumed to occur at a single node at the center of the beam. So, the function $R\langle t\rangle$ given by Eq. (6) is the only element in the load vector $\boldsymbol{R}$.

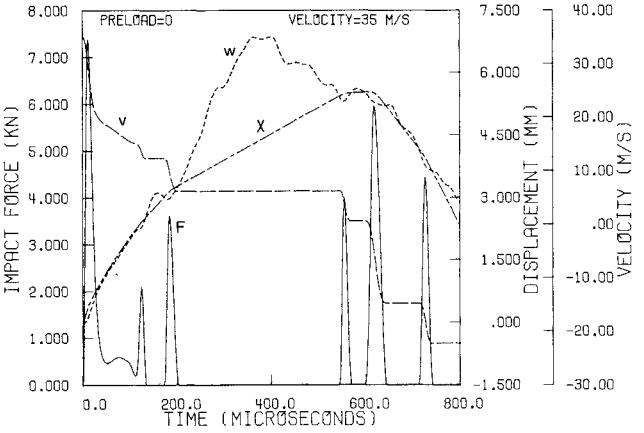

Fig. 2 Impact history, preload = 0.

Table 1 Properties of the composite beam and the impact parameters

Beam Dimensions	
Span	180 mm
Width	25.4 mm
Thickness	2.8 mm
Material	Graphite-epoxy
Layup	$[0_2/90_2/0_2/90_2/0_2]_s$
Boundary conditions	Clamped-clamped
Material Properties	
$E_1 = 130$ Gpa (18.89×10^6 psi)	
$E_2 = 12.9$ Gpa (1.87×10^6 psi)	
$G_{12} = 5.17$ Gpa (0.75×10^6 psi)	
$\nu_{12} = 0.24$	
Density $\rho = 1490$ kg/m^3 (1.392×10^{-4} lbf · s^2/in.^{4})	
Impact Parameters	
Impactor	12.7 mm diam steel ball
Impact mass	8.18 g
Impact velocity	15-35 m/s
Preload	0, 13.2, and 22 kN
Contact law	$F = k\alpha^2$ ($k = 1.293 \times 10^{11}$ N/m^2 $= 1.8744 \times 10^7$ lbf/in.^{2})
Unloading law exponent n_u	2.0
Reloading law exponent n_r	2.0

The application of a point load in the finite element model causes some convergence problems. This is because some of the stresses and displacements due to a concentrated load in the vicinity of the point of contact are singular.[14] So, as the finite element mesh is refined, these stresses diverge. This can be avoided by distributing the load over more than one node. But, this requires a knowledge of contact area at each instant of time during impact. Also, the number of elements required will be prohibitively large. So, in the present study, stresses and displacements at points away from the impact point were used as a check for convergence of the finite element solution. A time step of $\Delta T = 1$ μs in the Wilson-θ method was found to be satisfactory. It may be noted that the function $S(t)$ is the vertical displacement at the impact point due to the loading $R\langle t\rangle$. Similarly the $S^e(t)$ functions are the stresses at various points in the beam due to the dynamic load $R\langle t\rangle$. The S and S^e functions were computed for each time step and stored in a magnetic tape. The impact analysis was done for various combinations of velocities and initial stresses using the numerical algorithm, which has already been explained.

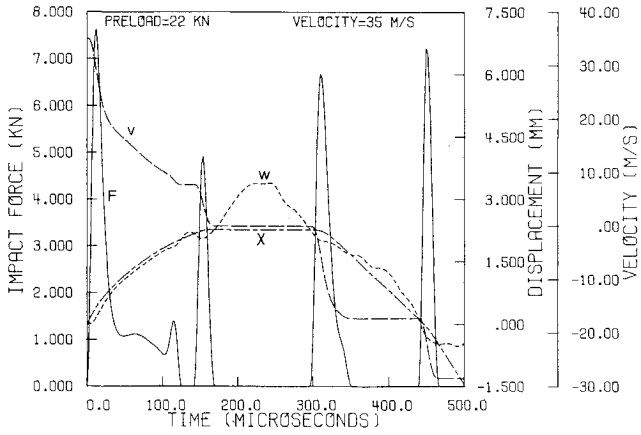

Fig. 3 Impact history, preload = 22 kN.

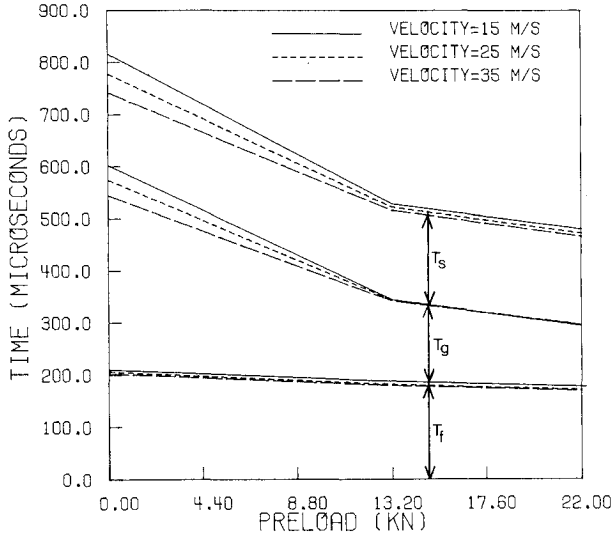

Fig. 4 Effect of preload on impact duration.

Effect of Initial Stresses on the Impact Response

As mentioned earlier, the results obtained in this analytical study may be considered as complementary to those presented in Ref. 9. The results show some interesting impact behavior that was not inferred before. It seems that impact responses depend closely on the impactor/structure combination, and the results presented here may be relevant only to the particular class of examples characterized by the various impact parameters used in this study.

The dimensions of the beam, material properties, and other impact parameters used in this study are listed in Table 1. The analyses were carried out for a beam without any preload and for beams under an axial tension of 13.2 and 22 kN. A previous analytical study[15] and experiments showed that the contact law is not very much affected by the presence of initial stresses. So, the contact law given in Table 1 was also used for the impact of initially stressed beams.

Impact Duration

Figure 2 shows a typical impact response when the beam is not preloaded. In the figure, F is the contact force, w the displacement of the beam at the impact point, χ the displacement of the impactor, and v the velocity of the impactor. It can be seen that the whole impact event lasts for a period of about 800 μs. The impactor is in contact with the beam during two distinct phases, which we may call as the first and second impact, respectively. The first impact occurs during the initial phase when the beam has not acquired sufficient velocity; this is followed by a period of loss of contact for a longer duration. As the beam reaches the maximum deflection point and returns, it hits the impactor again, causing the second impact. Even during the first (or second) phase of contact, we notice multiple impacts of shorter periods. Figure 3 gives the same information for a preloaded beam; it may be noted that the contact lasts for only about 480 μs.

Certain observations about the contact duration can be made from Fig. 4. The first and second contact durations, T_f and T_s, do not change very much with the impact velocity or the preload. The effect of preload is essentially to reduce the time of loss of contact T_g. This is not surprising because the natural frequencies of the preloaded beam are higher.

Impact Force

From Figs. 2 and 3 it may be seen that, generally, there are two force maxima, one during the first impact and the other during the second impact. Information on these force maxima are important, because the local contact stresses and the

Table 2 Kinetic energy of the impactor after the first and second impact

Impact velocity, m/s	Preload, kN	Velocity after 1st impact, m/s	Kinetic energy after 1st impact as % of impact energy	Velocity after 2nd impact, m/s	Kinetic energy after 2nd impact as % of impact energy
15	0	2.111	2.0	10.22	46
15	13.2	0.351	0.05	13.28	78
15	22.0	0.0259	0.00	10.15	46
25	0	4.048	2.6	17.26	48
25	13.2	0.731	0.09	21.63	75
25	22.0	0.0837	0.00	19.46	61
35	0	6.251	3.2	22.25	40
35	13.2	1.293	0.14	30.06	74
35	22.0	0.022	0.00	28.52	66

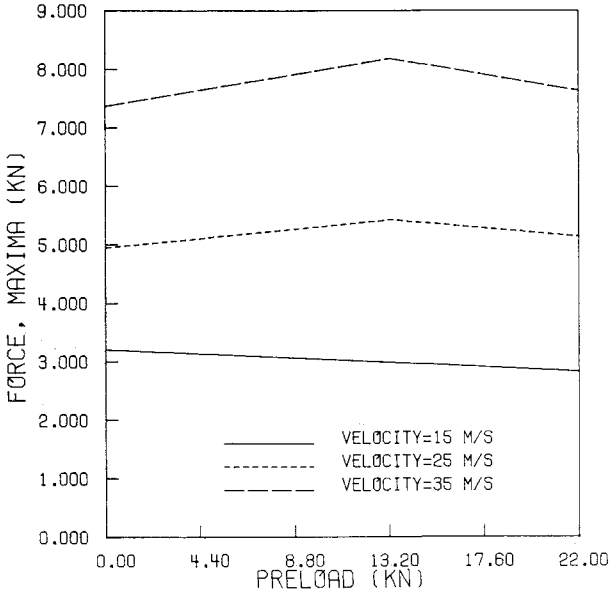

Fig. 5 Variation of maximum impact force with preload.

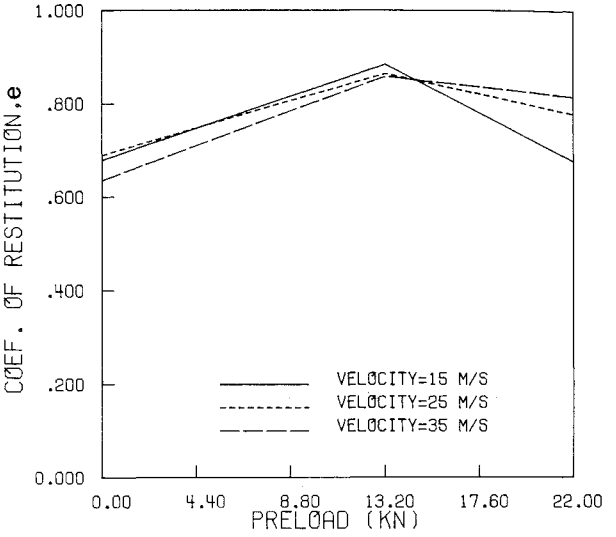

Fig. 6 Coefficient of restitution vs preload.

interlaminar shear stresses in the vicinity of the impact point depend very much upon the instantaneous contact force. The variation of maximum contact force with the preload is shown in Fig. 5. It is noted that in spite of considerable reduction in the total impact duration, the maximum force for a given impulse does not increase very much for the case of a preloaded beam. The obvious reason is that the reduction in impact duration is due to smaller T_g, whereas T_f and T_s remain almost the same.

Coefficient of Restitution

The coefficient of restitution e is a measure of the energy transferred to the structure during impact. From Fig. 6 it is seen that e is higher if the preload is present. It attains a maximum of about 0.87 when the preload is 13.2 kN. This means (see Table 2) that only 25% of the initial impactor energy is transferred to the beam, if there is a preload of 13.2 kN. Another quantity of interest is the velocity of the impactor after the first impact. It may be seen from Table 2 that the impactor loses almost all of its energy during the first impact.

Bending Stresses Due to Impact

The stresses were computed only at points considered to be crucial from the viewpoint of damage initiation. The bending stress σ_{xx} response history at a point P in the outer 90 deg layer (see Fig. 1) is discussed below.

Figure 7 presents the bending stresses for an impact velocity of 35 m/s in a beam free of initial stresses. The same information for a beam preloaded to a level of 22 kN is given in Fig. 8. It should be noted that in the case of a preloaded beam, the stresses plotted are incremental due to the impact. The actual normal stresses have to be obtained as the sum of the incremental and initial stresses. From these figures, it may be seen that the initial stress effect is negligible until $t = 50$ μs. If there is no preload, the maximum bending stress occurs at about $t = 625$ μs. In the case of the preloaded beam, the first maxima is the global maxima and occurs at about $t = 25$ μs.

The maximum total normal stresses at point P, i.e., sum of incremental bending and initial stresses, are plotted as a function of impact velocity in Fig. 9. The preload seems to have a stiffening effect on the beam, which reduces the incremental bending stresses for a given impact velocity. It may be seen that there is a velocity range over which the total normal stresses are less in the presence of initial stresses. Since such situations occur at high impact velocities, where the stress

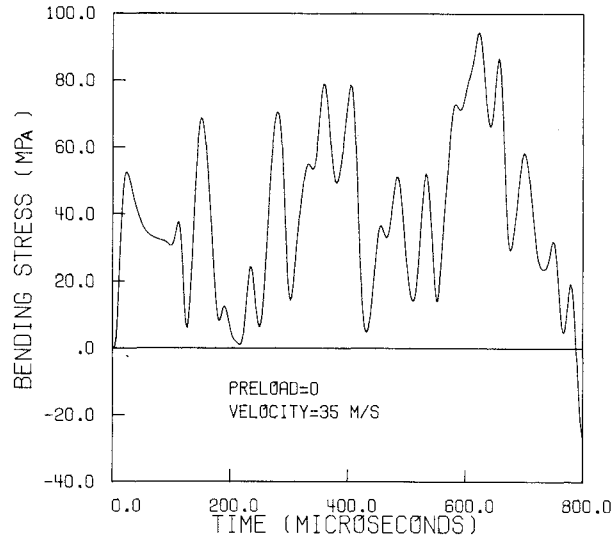

Fig. 7 Bending stresses at point P, preload = 0.

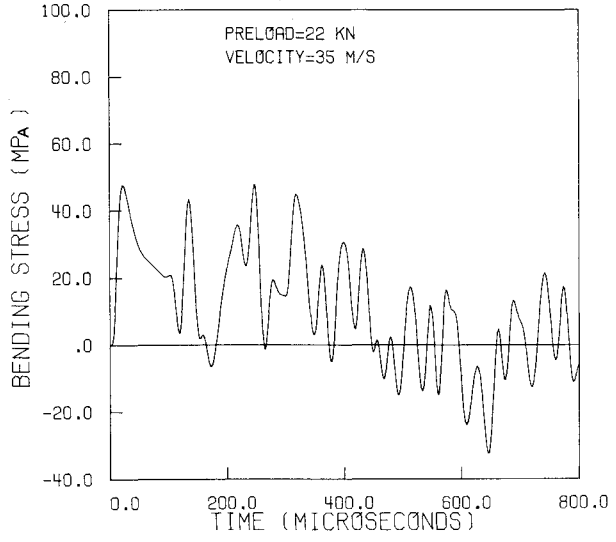

Fig. 8 Bending stresses at point P, preload = 22 kN.

levels are also higher, one good example of such beneficial effect of preload will be prevention of fiber breakage during impact.

Shear Stresses Due to Impact

The variation of maximum shear stresses at point Q and maximum impact force with the impact velocity is shown in Fig. 10. Both maximum shear stress and maximum impact force vary almost linearly with the impact velocity. The effect of preload is marginal. It was found that the maximum shear stress values were nearly equal to the shear stress at point Q due to a static load equal to the maximum impact force acting at the impact point.

The variation of shear stresses along the line PQ is shown in Fig. 11. Due to symmetry, the shear stresses at the center are identically equal to zero. They increase to a maximum at a distance from the center given by $X/L = 0.025$. The variation of shear stresses is similar at different impact velocities. Obviously, initial stresses tend to reduce the magnitude of the shear stresses.

Experimental Verification

Impact tests were performed on graphite-epoxy laminates to verify the response computed by analytical methods. The laminates were cured in the autoclave using SP 313 prepregs manufactured by 3M Company. The laminate configuration was $[0_2/90_2/0_2/90_2/0_2]_s$. The effective span of an impact specimen was 180 mm and the width 38 mm. The specimens were held by two rigid clamps on either side, which is assumed to simulate clamped-clamped boundary conditions. Initial tensile stresses were applied to the specimens by pulling them using a pneumatic cylinder. The description of the equipment can be found in Ref. 12.

A force transducer with a spherical cap was used as the impactor in this study. The impactor was attached to a thin rod that can swing about a shaft on bearings. The specifications of the force transducer and measurement techniques are discussed in Ref. 16. The impactor was dropped from a height such that the impact velocity was 2 m/s. The impact point was the center of the specimen. A strain gage was mounted on the longitudinal line of symmetry at a point 50 mm away from the center. The responses of the force transducer and the strain gage were stored in a waveform recorder (Gould Biomation 2805) and then plotted to a suitable scale.

Comparison of experimental results with the impact response computed using the finite element method are given in Figs. 12-15. It can be seen from Fig. 12 that our analysis is able to predict the multiple impacts observed in the tests. The results are in good agreement up to $t = 200$ μs. Thereafter a

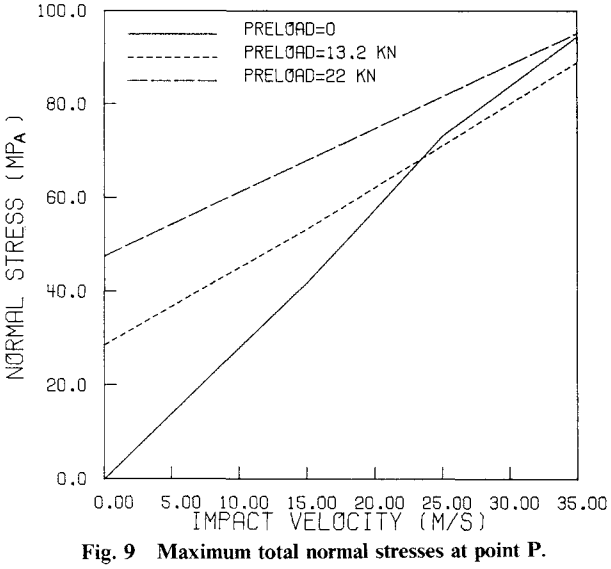

Fig. 9 Maximum total normal stresses at point P.

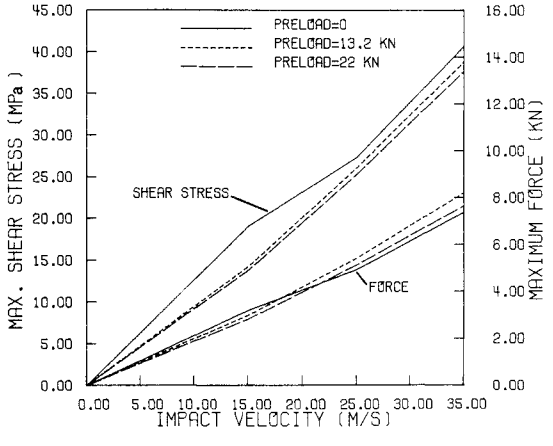

Fig. 10 Maximum shear stress at point Q.

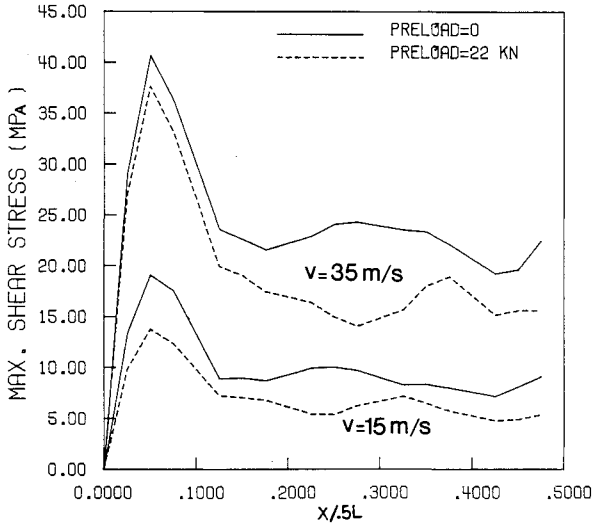

Fig. 11 Effect of preload on maximum shear stress.

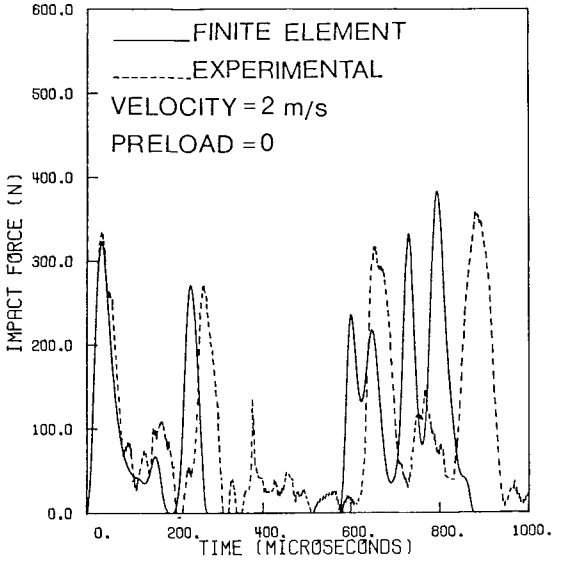

Fig. 12 Comparison of experimental and finite element results for impact force.

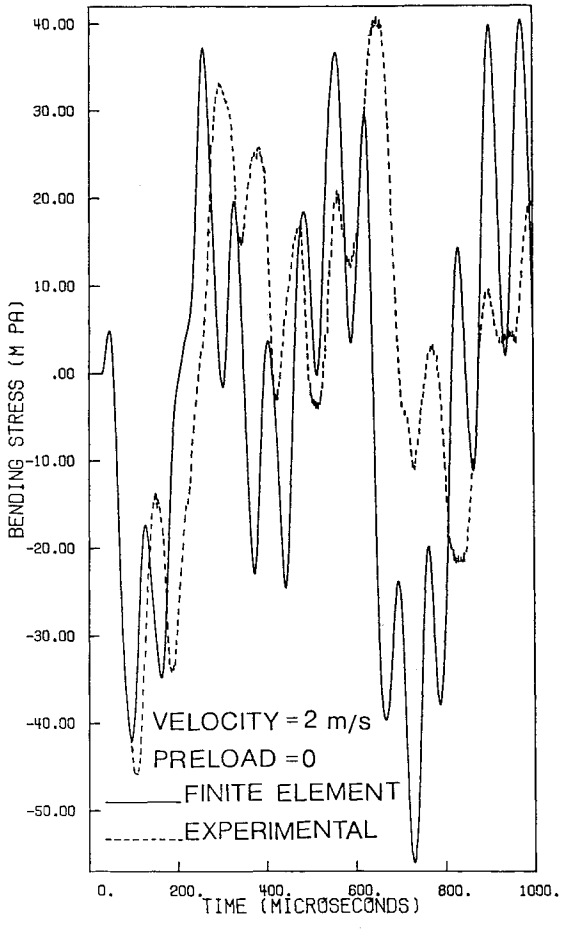

Fig. 13 Comparison of bending stresses.

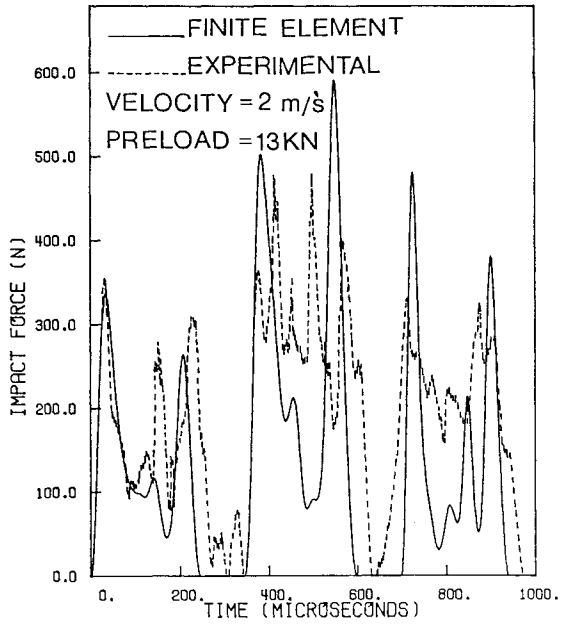

Fig. 14 Comparison of impact force on a preloaded beam.

phase shift occurs, although the prediction of the peak force values is reasonably good. Moreover, the duration of first and second impacts in the test results are about 12% more than that from the analysis. This discrepancy and also the phase shift suggest that the clamped-clamped boundary conditions might not have been completely realized in the impact tests.

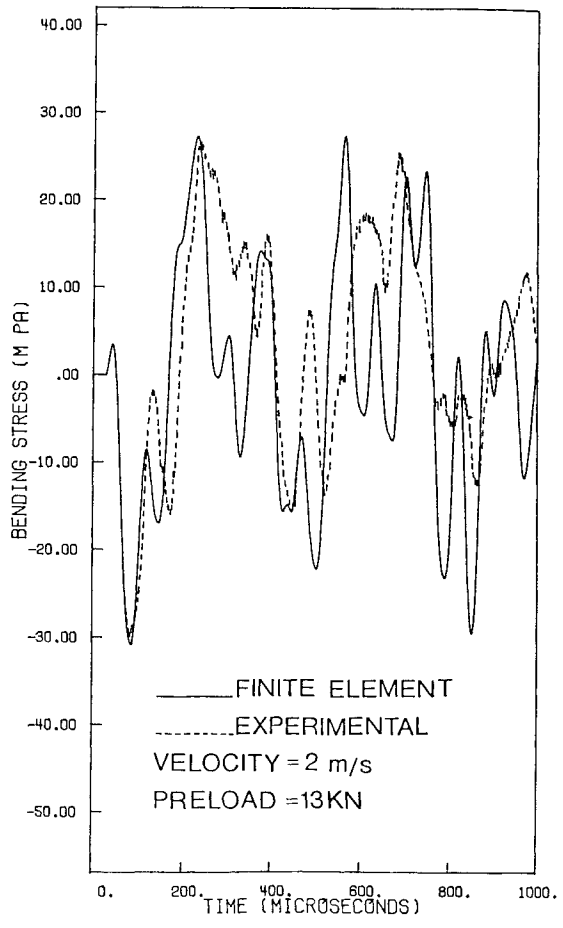

Fig. 15 Comparison of bending stresses in a preloaded beam.

When the beam is under preload, the discrepancy in phase shift shown in Fig. 14 is less. But, the prediction of higher impact forces indicates that the finite element beam model is stiffer than the actual test specimen. Similar observations can be made with the stress response results presented in Figs. 13 and 15.

Summary and Conclusions

Finite element methods in conjunction with an efficient numerical algorithm were used to study the impact response of a graphite-epoxy laminated beam for various combinations of impact velocities and preloads. The analyses predict multiple impacts. The tensile initial stresses reduce the impact duration; the reduction is mainly due to the decrease in the period of loss of contact in between multiple impacts. The maximum impact force is not very much affected by the preload. Initial tensile stresses reduce the incremental bending stresses due to impact. But, depending on the impact velocity, the total normal stresses, i.e., the sum of initial stresses and incremental bending stresses, may be greater or less than the bending stresses in a beam without any preload. The tensile initial stresses also reduce the maximum interlaminar shear stresses. This suggests that the preload may reduce the likelihood of delamination, and consequently, the damage.

Low-velocity impact tests were conducted using a force transducer as a pendulous impactor. The experiments verified the multiple impacts predicted by the finite element methods. Experimental force and strain histories agreed well with the finite element computations.

Acknowledgment

This work was supported by NASA Langley Research Center Grant NAG 1222 with Purdue University. The authors thank

Prof. James F. Doyle for his useful discussion of the experimental part of the work.

References

[1]*Foreign Object Impact Damage to Composites*, ASTM STP 568, 1973.

[2]Lee, E.H., "The Impact of a Mass Striking a Beam," *Journal of Applied Mechanics*, Vol. 7, 1940, pp. A129-A138.

[3]Goldsmith, W., *Impact*, Edward Arnold, London, 1960, pp. 109-111.

[4]Sun, C.T. and Huang, S.N., "Transverse Impact Problems by Higher Order Beam Finite Elements," *Computers and Structures*, Vol. 5, 1975, pp. 297-303.

[5]Elber, W., "Failure Mechanics in Low-Velocity Impacts on Thin Composite Plates," NASA TP 2152, 1983.

[6]Yang, S.H. and Sun, C.T., "Indentation Law for Composite Laminates," ASTM STP 787, 1982, pp. 425-449.

[7]Butcher, B.R., "The Impact Resistance of Unidirectional CFRP Under Tensile Stress," *Fibre Science and Technology*, 1979, pp. 295-326.

[8]Butcher, B.R. and Fernback, P.J., "Impact Resistance of Unidirectional CFRP Under Tensile Stress: Further Experimental Variables," *Fibre Science and Technology*, 1981, pp. 41-58.

[9]Sun, C.T. and Chattopadhyay, S., "Dynamic Response of Anisotropic Laminated Plates Under Initial Stresses to Impact of Mass," *Journal of Applied Mechanics*, Vol. 42, 1975, pp. 683-698.

[10]Sankar, B.V. and Sun, C.T., "An Efficient Numerical Algorithm for Transverse Impact Problems," *Computers and Structures*, to be published.

[11]Zienkiewicz, O.C., *The Finite Element Method*, McGraw-Hill Book Co., New York, 1977, pp. 500-504.

[12]Sankar, B.V., "Contact Behavior, Impact Response and Damage in Graphite-Epoxy Laminates Subjected to Initial Stresses," Ph.D. Thesis, Purdue University, West Lafayette, IN, May 1984.

[13]Bathe, K.J. and Wilson, E.L., *Numerical Methods in Finite Element Analysis*, Prentice-Hall, Englewood Cliffs, NJ, 1976.

[14]Timoshenko, S.P. and Goodier, J.N., *Theory of Elasticity*, McGraw-Hill Book Co., New York, 1970, pp. 113-116.

[15]Sun, C.T. and Sankar, B.V., "Contact Between a Rigid Cylinder and an Orthotropic Beam Under Initial Stresses," *1982 Advances in Aerospace Structures and Materials*, edited by R.M. Laurenson and U. Yuceoglu, ASME Pub. AD-03, Nov. 1982, pp. 37-45.

[16]Tan, T.M., "Wave Propagation in Graphite-Epoxy Laminates Due to Impact," Ph.D. Thesis, Purdue University, West Lafayette, IN, 1982.